Theoretical investigations of collision dynamics of cytosine by low-energy (150–1000 eV) proton impact*

Zhi-Ping Wang(王志萍)[1,†], Feng-Shou Zhang(张丰收)[2], Xue-Fen Xu(许雪芬)[1], and Chao-Yi Qian(钱超义)[1]

[1] *Department of Fundamental Courses, Wuxi Institute of Technology, Wuxi* 214121, *China*

[2] *The Key Laboratory of Beam Technology and Material Modification of Ministry of Education, College of Nuclear Science and Technology, Beijing Normal University, Beijing* 100875, *China*

(Received 7 October 2019; revised manuscript received 12 December 2019; published online 18 December 2019)

Using a real-space real-time implementation of time-dependent density functional theory coupled to molecular dynamics (TDDFT-MD) nonadiabatically, we theoretically study both static properties and collision process of cytosine by 150–1000 eV proton impact in the microscopic way. The calculated ground state of cytosine accords well with experiments. It is found that proton is scattered in any case in the present study. The bond break of cytosine occurs when the energy loss of proton is larger than 22 eV and the main dissociation pathway of cytosine is the breaks of C_1N_2 and N_8H_{10}. In the range of 150 eV $\leq E_k \leq$ 360 eV, when the incident energy of proton increases, the excitation becomes more violent even though the interaction time is shortened. While in the range of 360 eV $< E_k \leq$ 1000 eV, the excitation becomes less violent as the incident energy of proton increases, indicating that the interaction time dominates mainly. We also show two typical collision reaction channels by analyzing the molecular ionization, the electronic density evolution, the energy loss of proton, the vibration frequency and the scattering pattern detailedly. The result shows that the loss of electrons can decrease the bond lengths of C_3N_8 and C_5N_6 while increase the bond lengths of C_4H_{11}, C_5H_{12} and C_4C_5 after the collision. Furthermore, it is found that the peak of the scattering angle shows a little redshift when compared to that of the loss of kinetic energy of proton.

Keywords: time-dependent density functional theory, cytosine, collision, proton

PACS: 34.50.Gb, 82.30.Fi, 87.15.H– **DOI:** 10.1088/1674-1056/ab6313

1. Introduction

It is known that the interaction of DNA with ionizing particles is a very complex process and DNA is the most important target radiation as the single- and double-strand breaking in DNA can cause mutation.[1–5] Nucleic acid bases are the basic building blocks of DNA, therefore understanding their properties is crucial. In the past decades, many efforts have been devoted to investigating the physico-chemical processes resulting from the interaction of ionizing radiation with DNA and nucleic acid bases experimentally and theoretically.[6–15] Such a work aims to understanding the elementary reactive processes occurring during the initial radiation attack and afterwards at the molecular level. Cytosine is one of the simplest pyrimidine bases and is a basic component of DNA and RNA acids. Chen *et al.* determined the adiabatic ionization energies of specific gas-phase cytosine tautomers produced in a molecular beam.[16] Trofimov *et al.* investigated the complete valence shell photoelectron spectra of cytosine experimentally and theoretically.[17] The fragmentation of cytosine has been experimentally studied by mass spectroscopy in gas phase by proton impact,[9,18] photoionization,[7,8] and electron impact.[19,20] In literature, theoretical studies on the detailed microscopic collision process of cytosine are very few to date.

In this work, we explore the electronic and vibronic excitations of cytosine impacted by proton in the microscopic way. Our calculations are based on the approach of the time-dependent density functional theory (TDDFT) coupled to molecular dynamics non-adiabatically. The TDDFT-MD approach implemented in the code package PWTELEMAN used here is developed by the Toulouse–Erlangen group.[21–24] It has been applied as an effective tool in exploring ion-molecule collision dynamics,[25–30] nonlinear dynamics in metal and water clusters, and biomolecules.[22,23,31–33] Encouraged by these successful study with TDDFT-MD, we are devoted to investigate the influence of the incident energy of proton on the collision process of cytosine.

It should be noted that for a more precise understanding of collision, it is necessary to take a complete study considering the incidence directions and the charge state of the projectile, impact parameters and energies. However, this is not computationally feasible yet. Thus, the detailed study of the incidence direction and impact parameters is out of the scope of this work. It is known that when a target is collided with a projectile with low energies, there will be appearance of some phenomena in the collision process, such as charge transfer, nuclear exchange, vibration excitation, dissociation, etc. Thus, we concentrate on exploring the effect of the kinetic energy of projectile on the collision dynamical process for proton with

*Project supported by the National Natural Science Foundation of China (Grant Nos. 11905160 and 11635003) and the Natural Science Foundation of Jiangsu Province of China (Grant No. BK20160199).

†Corresponding author. E-mail: zpwang03247@163.com

initial kinetic energy ranging from 150 eV to 1000 eV, which belongs to the low energy region.

The organization of this paper is as follows. In Section 2, we give a brief explanation of the theoretical and numerical approach. In Section 3, we discuss the calculated results. Finally, a summary is presented in Section 4.

2. Theory and simulation details

We use the same approach applied in our previous study.[28,31] We give a brief summary here. In TDDFT-MD, the system is described as an ensemble composed of valence electrons and ions. For an ion, it is composed of the inner shell electrons and their parent nuclei. Thus, for cytosine, it owns 42 valence electrons and 14 ions. The degrees of freedom of the system are the wave functions of valence electrons $\varphi_j(\boldsymbol{r})$ $(j=1,\ldots,N_{\rm el})$, where $N_{\rm el}$ is the total number of valence electrons, and the coordinates of the system's ionic cores $\boldsymbol{R}_I$ $(I=1,\ldots,N_{\rm ion})$, where $N_{\rm ion}$ is the total number of ions.

The total energy of system is given as follows:

$$\begin{aligned} E_{\rm tot} &= E_{\rm kin,el}(\{\varphi_j\})+E_{\rm C}(\rho)+E_{\rm xc}(\rho)+E_{\rm SIC}(\{|\varphi_j|^2\}) \\ &\quad +E_{\rm kin,ion}(\{\dot{\boldsymbol{R}}_I\})+E_{\rm pot,ion}(\{\boldsymbol{R}_I\}) \\ &\quad +E_{\rm PsP}(\{\varphi_j\},\{\boldsymbol{R}_I\})+E_{\rm ext}, \end{aligned} \tag{1}$$

where $\rho(\boldsymbol{r},t)$ is the electron density given by $\rho(\boldsymbol{r},t)=\sum_j|\varphi_j(\boldsymbol{r},t)|^2$. In Eq. (1), $E_{\rm kin,el}$ is the electron kinetic energy, $E_{\rm C}$ denotes the direct Coulomb energy, $E_{\rm xc}$ represents the exchange-correlation energy and $E_{\rm SIC}$ is the self-interaction correction term. $E_{\rm kin,ion}$, $E_{\rm pot,ion}$, $E_{\rm PsP}$, and $E_{\rm ext}$ denote the ion kinetic energies, the ion potential, the pseudo-potential, and the external energy, respectively.

We perform real-time propagation of electron wave functions on the basis of TDDFT. The time evolution of the electronic wave function is achieved employing a set of time-dependent Kohn–Sham (TDKS) equations,[34] given as

$$\mathrm{i}\frac{\partial}{\partial t}\varphi_j(\boldsymbol{r},t) = \left(-\frac{\nabla^2}{2}+V_{\rm eff}[\rho(\boldsymbol{r},t)]\right)\varphi_j(\boldsymbol{r},t). \tag{2}$$

Here $V_{\rm eff}$ is the time-dependent Kohn–Sham potential

$$\begin{aligned} V_{\rm eff}[\rho(\boldsymbol{r},t)] &= V_{\rm ne}(\boldsymbol{r},t)+V_{\rm H}[\rho(\boldsymbol{r},t)]+V_{\rm xc}[\rho(\boldsymbol{r},t)] \\ &\quad +V_{\rm ext}(\boldsymbol{r},t), \end{aligned} \tag{3}$$

where $V_{\rm ne}$ is the electron–ion potential, $V_{\rm H}$ is the Hartree potential, $V_{\rm xc}$ is the exchange–correlation potential, and $V_{\rm ext}(\boldsymbol{r},t)$ is the external potential.

The ion motion is obtained by using molecular dynamics (MD) simulations. The equations of motion can be obtained by variations of ionic position $\boldsymbol{R}_I$ and momentum $\boldsymbol{P}_I$, given as

$$\frac{\partial}{\partial t}\boldsymbol{R}_I=\frac{\boldsymbol{P}_I}{M_I}, \tag{4}$$

$$\begin{aligned} \frac{\partial}{\partial t}\boldsymbol{P}_I &= -\nabla_{R_I}\Big[\frac{1}{2}\sum_{I\neq J}\frac{Z_IZ_J}{|\boldsymbol{R}_I-\boldsymbol{R}_J|}+\sum_{i=1}^{N_{\rm el}}\langle\varphi_j|V_{\rm PsP}(\boldsymbol{r}-\boldsymbol{R}_I)|\varphi_j\rangle \\ &\quad +V_{\rm ext,ion}(\boldsymbol{R}_I,t)\Big], \end{aligned} \tag{5}$$

where M_I and Z_I are the mass and the charge of the ion number I. $V_{\rm PsP}$ and $V_{\rm ext,ion}$ represent the pseudo-potential and the interaction between ions and the external field, respectively.

The dynamical Eqs. (2), (3) and (4) for electrons and ions are computed and solved simultaneously, and both electrons and ions are fully propagated in time. The coupling between electrons and ionic cores is mediated by Goedecker-type pseudopotentials.[35] The parameterization of Perdew and Wang[36] is applied for $E_{\rm xc}$. An average-density self-interaction correction (ADSIC)[37] is employed to put the single-particle energies at their correct values.

In the present study, all calculations are performed on a 3D coordinate-space grid of $96\times96\times96$. The grid spacing is $0.412a_0$ in each direction. The damped gradient method[22] is applied to get the ground state wavefunctions of the system. A constant time step for propagation of the wave function and ionic motion is 0.000605 fs to ensure the numerical stability. The absorbing boundary condition is applied to avoid periodic reflecting electrons.[38]

To describe electronic excitation, the number of bound electrons $N(t)$, which is associated with the time-dependent electronic density $\rho(\boldsymbol{r},t)$ within the finite volume V, is given as

$$N(t)=\int_V \mathrm{d}\boldsymbol{r}\rho(\boldsymbol{r},t). \tag{6}$$

Accordingly, the number of escaped electrons can be defined as $N_{\rm esc}(t)=N(t=0)-N(t)$. The scattering angle θ is applied to describe the interaction of projectile and target. It is defined as the angle between the scattered and incident directions, which is given as[39]

$$\cos\theta=P/|\boldsymbol{P}|, \tag{7}$$

where P is the final momentum component of the outgoing proton along the initial incident direction, and $\boldsymbol{P}$ is the final total momentum of the outgoing proton.

3. Results and discussion

3.1. Ground state calculation of cytosine

Cytosine is one of the four main bases found in DNA and RNA. It is a pyrimidine derivative, with a heterocyclic aromatic ring and two substituents attached. Figure 1 shows the optimized ground state configuration of cytosine. There are three double bonds, C_1O_7, N_2C_3 and C_4C_5 in cytosine. The right panel in Fig. 1 shows the contour plot of the electronic density of cytosine in xy plane, indicating that ions are concentrated well around by electrons. Table 1 gives both the experimental and calculated values for the geometrical parameters of cytosine. The relative errors are also listed.

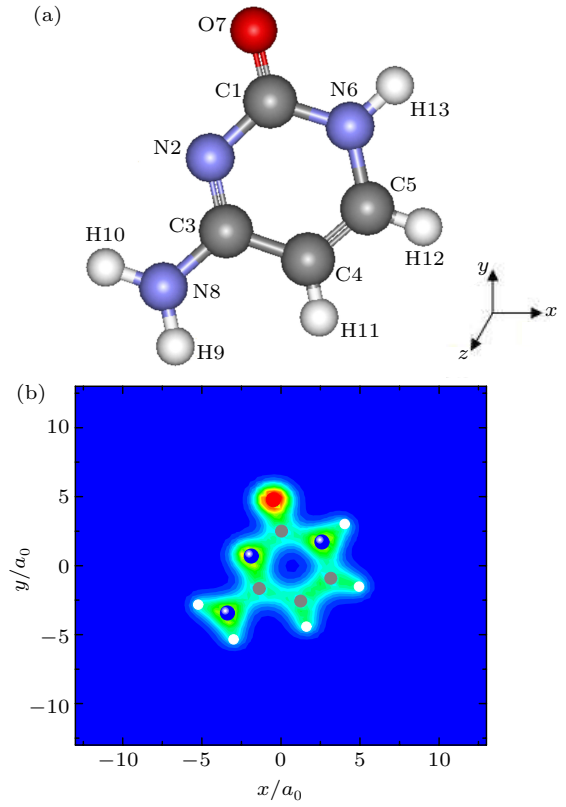

Fig. 1. (a) Optimized molecular structure of cytosine, showing the atomic numbering, and (b) the contour plots of the electronic density of cytosine in the *xy* plane. Full red, blue, grey and white circles stand for oxygen, nitrogen, carbon and hydrogen ions, respectively.

Table 1. Optimized geometrical parameters of cytosine. Bond lengths are in units of a_0 and angles are in units of degree.

Parameter	Expt.[40]	This work	Err	B1LYP/6-311G(d,p)[41]
$R(C_1N_6)$	2.589	2.650	2.4%	2.700
$R(C_1N_2)$	2.570	2.618	1.9%	2.591
$R(N_2C_3)$	2.532	2.490	1.7%	2.483
$R(C_3C_4)$	2.683	2.708	0.9%	2.723
$R(C_4C_5)$	2.532	2.512	0.8%	2.561
$R(C_5N_6)$	2.570	2.584	0.6%	2.557
$R(C_1O_7)$	2.324	2.336	0.6%	2.288
$R(C_3N_8)$	2.513	2.588	3%	2.570
$R(N_6H_{13})$		1.901		1.905
$R(N_8H_9)$		1.807		1.903
$R(N_8H_{10})$		1.777		1.898
$R(C_4H_{11})$		1.890		2.039
$R(C_5H_{12})$		1.890		2.044
$\theta(N_2C_1N_6)$	118	119.4	1.2%	115.9
$\theta(C_1N_2C_3)$	120	121.0	0.9%	120.5
$\theta(N_2C_3C_4)$	122	121.2	0.7%	124.1
$\theta(C_3C_4C_5)$	117	120.1	2.7%	116.0
$\theta(C_4C_5N_6)$	120	119.0	0.9%	120.0
$\theta(C_5N_6C_1)$	123	119.1	0.8%	123.4
$\theta(N_6C_1O_7)$	120	120.3	0.3%	118.3
$\theta(N_2C_1O_7)$	122	120.2	1.9%	125.8
$\theta(N_2C_3N_8)$	118	119.4	1.2%	117.1
$\theta(C_4C_3N_8)$	120	119.4	0.5%	118.8
$\theta(H_{10}N_8H_9)$		120.1		118.5

In Table 1, the calculated typical bond lengths and angles of cytosine are in good agreement with the experimental results.[40] The calculated ionization potential, which is corresponding to the energy of the last occupied electron state of cytosine is 8.85 eV. It agrees well with the experimental value 8.94 eV[42] with a 1.0% discrepancy. These make us believe that the calculated results of the ground state of cytosine are acceptable.

3.2. Collision setup

Now we turn to study the proton-cytosine collision problem to see how a cytosine evolves during and after the impact of an energetic proton. As cytosine is a planar molecule, we consider that proton moves in the plane of cytosine toward the C_5N_6 single bond and the center of mass of cytosine. Figure 2 displays the collision configuration. Cytosine is placed in the cuboid box and the center of mass is in the origin. The proton moves along the *x* direction from the initial position ($20a_0$, 0, 0). In the present study, after systematic analysis, we find that the proton is scattered away in all situations. In addition, as the incident energy of proton belongs to the low energy region, it is found that the primary mechanism of target ionization is electron capture, which accords well with the results found by Yu *et al.*[26] To have a profound and direct dynamical understanding of collision dynamics, we analyze two cases in detail, which are $E_{k0} = 200$ eV and $E_{k0} = 300$ eV.

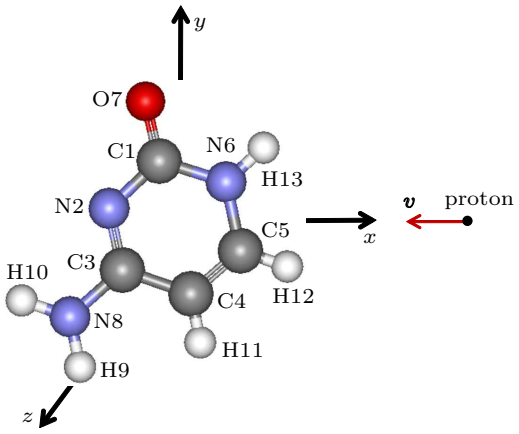

Fig. 2. The setup of proton-cytosine collision. The center of mass of target is initially in the origin.

Figure 3 shows the time evolution of the ionic positions of proton and ions in the ring of cytosine in the *x* direction for $E_{k0} = 200$ eV and $E_{k0} = 300$ eV, respectively. In the case of $E_{k0} = 200$ eV, as shown in Fig. 3(a), proton approaches C_5 at around 2.8 fs, then penetrates the ring in 1.5 fs. When the proton leaves the cytosine at around 4.4 fs, it changes the direction of motion and the scattering angle is about 58.9°. In the whole duration of collision, the ions in the ring of cytosine keep on the gentle vibration. In Fig. 3(b), in the case of $E_{k0} = 300$ eV, proton penetrates into the ring of cytosine first, then it is rebounded before attaching N_2 and the scattering angle attains about 100°. The N_2 is scattered at about 3 fs and moves directly toward the boundary of computational box, indicating the breaking of the heterocyclic aromatic ring of cytosine.

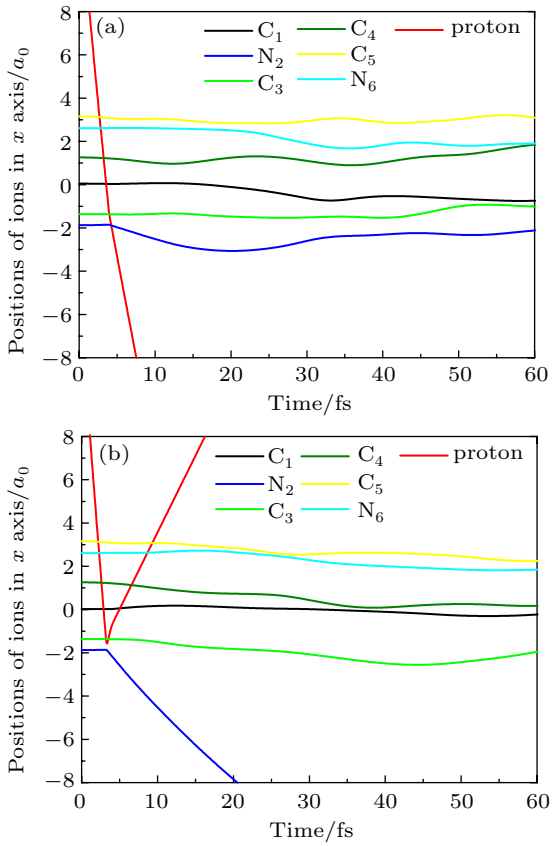

Fig. 3. The time evolution of ionic positions of proton and ions in the ring of cytosine in the x direction (a) for $E_{k0} = 200$ eV and (b) for $E_{k0} = 300$ eV.

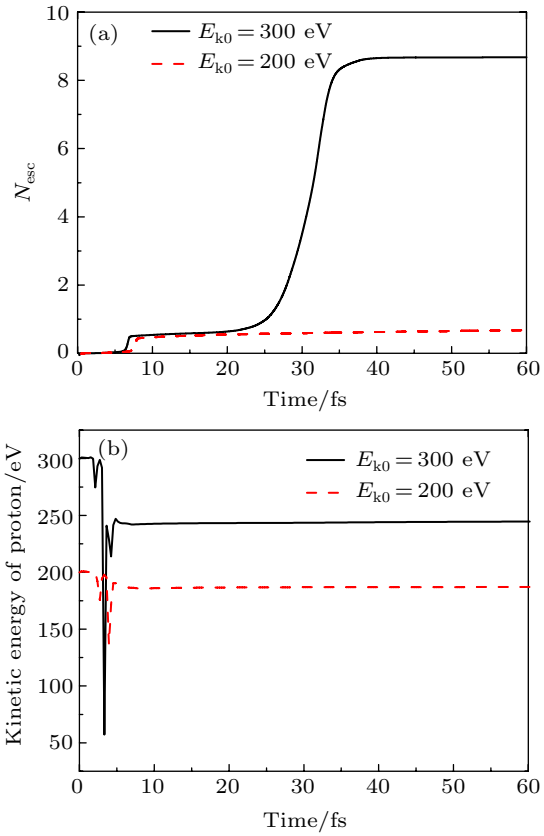

Fig. 4. The time evolutions of the ionization of cytosine (a) and the kinetic energy of proton (b) for the same cases shown in Fig. 3.

Figures 4(a) and 4(b) show the time evolutions of the ionization of cytosine and the kinetic energy of proton for the same cases in Fig. 3. In the case of $E_{k0} = 200$ eV, as shown in Fig. 4(a), the ionization of cytosine takes place at around 7.3 fs and increases quickly in a short time. It attains the saturate value 0.45 at around 8.22 fs. This means that cytosine loses about 0.45 electrons during the collision. Comparing the time scale in Figs. 3(a) and 4(a), one can find that the ionization takes place later than the moment when the proton is closest to cytosine. This is due to the fact that 0.45 electrons are captured by proton and the ionization takes place when proton moving toward the boundary of computational box. This could be further understood by considering the time-dependent electron density, and a few snapshots are shown in Fig. 5. After being crossed by proton, the C_5N_6 bond shows small deformation ($t = 3.025$ fs). Then, proton moves toward the boundary of box with some captured electrons ($t = 6.05$ fs). In the remaining time, cytosine keeps on vibration and the remaining electrons couple well with ions. For the kinetic energy of proton, as seen from the red dashed line in Fig. 4(b), owing to the medium-range polarization interaction, it decreases first and then increases a little when the proton attaches the bond C_5N_6. Then as the proton penetrates into the ring of cytosine, the same variation trend of E_k occurs twice again. Finally, proton loses about 12.97 eV, which is 6.5% of E_{k0}.

In the case of $E_{k0} = 300$ eV, in first 20 fs, the variation of ionization is similar to that in the case of $E_{k0} = 200$ eV except the earlier appearance of ionization. The proton captures about 0.5 electrons during the collision. However, from about 20 fs, the ionization starts to increase again and 8.1 more electrons are lost until 38 fs. This is caused by the departure of N_2 and H_{10} accompanied with electrons. This could also be further understood by considering the snapshots of the evolving process as shown in Fig. 6. At $t = 3.025$ fs, proton attains the N_2 after crossing the C_5N_6 bond. Then it is immediately scattered away carrying the captured electrons. At the same time, the C_1N_2 bond is broken. This agrees with the result that the loss of electrons weakens the C_1N_2 double bond in cytosine.[41,43] Then, N_2 ion, which gains about the kinetic energy of 25 eV, moves toward H_{10} inducing the broken of N_8H_{10} (see the snapshot of $t = 15.125$ fs). Finally, N_2 and H_{10} accompanied with electrons depart from cytosine and move away directly from the computational box. This exhibits well the production of secondary species along the radiation track which can further react within irradiated cells. In the remaining time, the remaining part of cytosine keeps on vibration and rotation. Although the variation of the kinetic energy of proton (the black solid line in Fig. 4(b)) is similar to that in the case of $E_{k0} = 200$ eV, proton loses about 55.74 eV, which is much more than that in the case of $E_{k0} = 200$ eV.

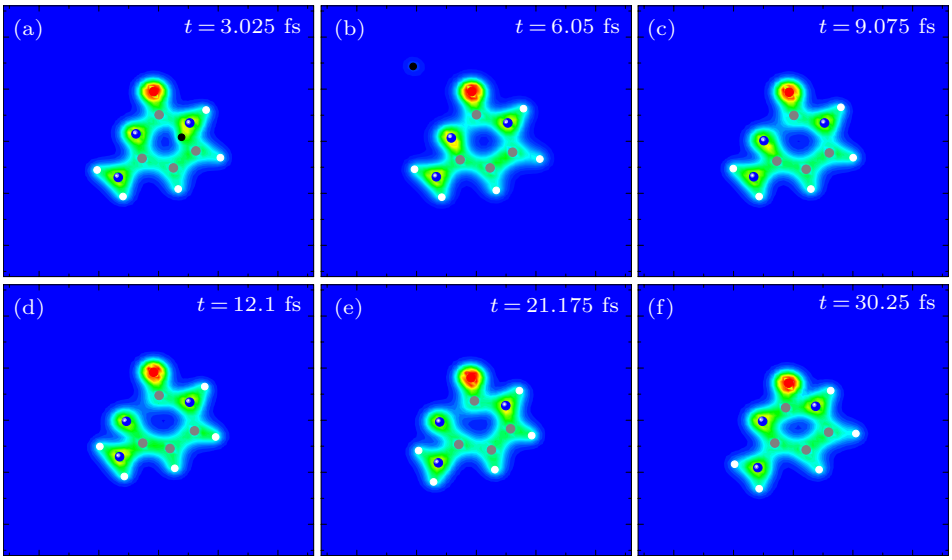

Fig. 5. Eight snapshots of the evolving process of proton impacting with cytosine in the case of $E_{k0} = 200$ eV. Full red, blue, grey and white circles are oxygen, nitrogen, carbon and hydrogen atoms, respectively. The black circle represents the proton.

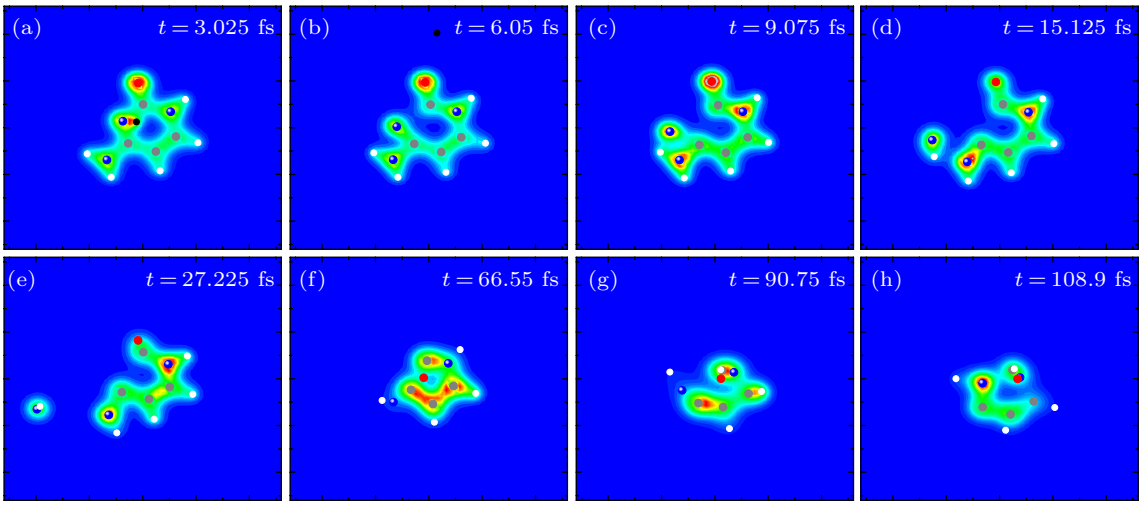

Fig. 6. Eight snapshots of the evolving process of proton impacting with cytosine in the case of $E_{k0} = 300$ eV. Full red, blue, grey and white circles stand for oxygen, nitrogen, carbon and hydrogen atoms, respectively. The black circle represents the proton.

Here we turn to discuss the deformation and vibration behavior of cytosine during the collision. Figures 7 and 8 show the time evolution of the atomic distances of cytosine in the case of $E_{k0} = 200$ eV and $E_{k0} = 300$ eV, respectively. It is obvious that cytosine shows an inter-ion vibration behavior in both cases. In the case of $E_{k0} = 200$ eV, as shown in Figs. 7(a) and 7(b), the bonds keep on vibration before and after collision. Although the bond C_1N_2 is enlarged immediately after the closest approach, it remains unbroken in the remaining time. This is due to the fact that N_2 does not gain enough kinetic energy to move away. In the case of $E_{k0} = 300$ eV, one can see from Figs. 8(a) and 8(b) that C_1N_2 breaks first followed by breaks of N_2C_3 and N_8H_{10}. In both the two cases, the bonds C_3N_8 and C_5N_6 are shortened while C_4H_{11}, C_5H_{12} and C_4C_5 are enlarged after the collision. This accords well with the result found by Tehrani *et al.*[43] that the ionization could lead to the decreases of the lengths of C_3N_8 and C_5N_6, whereas lead to the increase of the lengths of N_2C_3 and C_4C_5 bonds.

One can also estimate the vibration frequencies of cytosine after the collision from Figs. 7 and 8. The estimated results are exhibited in Table 2. The corresponding experimental results of cytosine explored by Radchenko *et al.*[44] and Susi *et al.*[45] are also given. Radchenko *et al.* obtained high-resolution vibrational spectra of cytosine through IR spectroscopy in an Ar matrix.[44] Susi *et al.* obtained the laser-Raman spectra and IR spectra of polycrystalline cytosine.[45] Comparing the results in Table 2, one can find that the stretching vibration frequencies of C_1O_7, N_2C_3 and C_3N_8 are increased after the collision, while the frequencies $\nu(C_4C_5)$, $\nu(C_4H_{11})$, $\nu(C_5H_{12})$, $\nu(C_6H_{13})$ and $\nu(N_8H_{10})$ are decreased. Furthermore, the more violent the collision, the greater the change of vibration frequency.

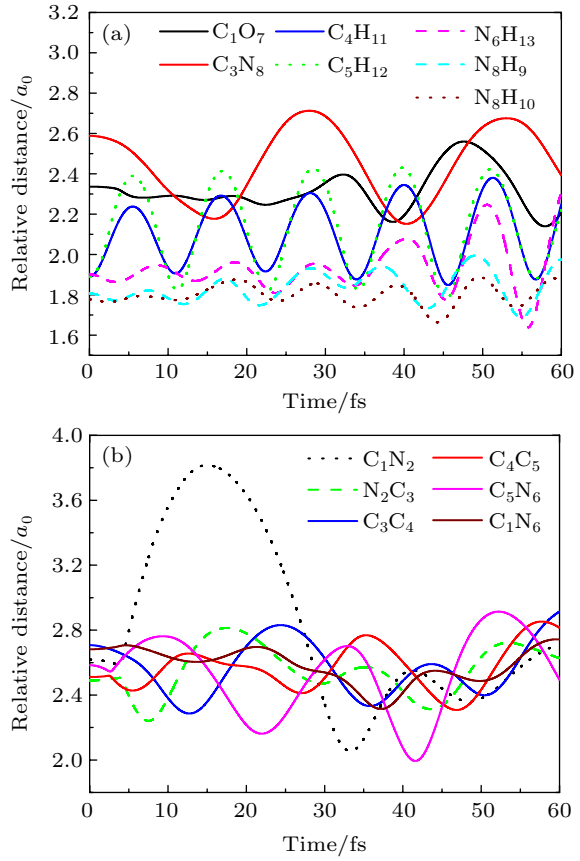

Fig. 7. The atomic distances of cytosine as a function of time in the case of $E_{k0} = 200$ eV.

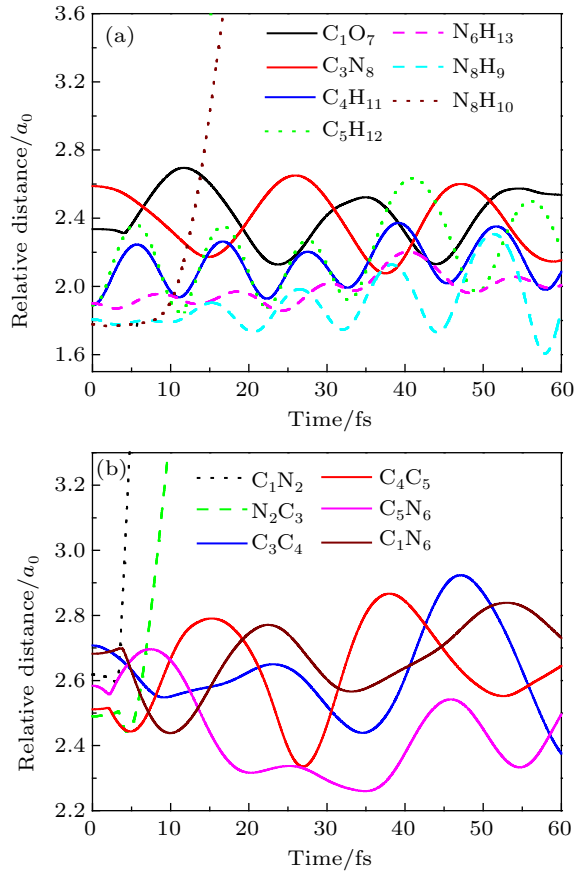

Fig. 8. The atomic distances of cytosine as a function of time in the case of $E_{k0} = 300$ eV.

Table 2. Calculated frequencies of stretching mode of cytosine after collision in the cases of $E_{k0} = 200$ eV and $E_{k0} = 300$ eV (in cm^{-1}). The corresponding experimental results of cytosine in the ground state are also given.

Type of vibration	Expt.[44]	$E_{k0} = 200$ eV	$E_{k0} = 300$ eV
$\nu(C_1O_7)$	1714	1737	1772
$\nu(N_2C_3)$	1595	1960	
$\nu(C_4C_5)$	1655	1533	1293
$\nu(C_3N_8)$	1318	1332	1572
$\nu(C_5N_6)$	1450[45]	1689	1673
$\nu(C_4H_{11})$	3117[45]	2942	2607
$\nu(C_5H_{12})$	3117[45]	2895	2199
$\nu(N_6H_{13})$	3468	3200	2499
$\nu(N_8H_{10})$	3438	3261	2720

We present the energy loss of proton together with the scattering angle as a function of the incident energy of proton ranging from 150 eV to 1000 eV in Fig. 9. One can find that both the proton energy loss ΔE_k and the scattering angle θ depend strongly on the incident energy of proton. When the incident energy ranges from 150 eV to 1000 eV, both ΔE_k and θ show the same trend of variation, which increases firstly, then attains the maximum, and decreases later. With respect to ΔE_k, in the absolute term, it ranges from 6.92 eV to 93.39 eV and the maximum peaks at $E_k = 390$ eV approximately. For the scattering angle θ, it varies from 10.94° to 163.3° and the maximum appears at $E_k = 360$ eV. It is obvious that the peak of ΔE_k shows a little blue shift when compared to that of the scattering angle. This could be attributed to the fact that the scattering angle is mainly affected by head-on impact, while the electron density is higher in the chemical bond region and the proton's interaction with the electrons is expected to be stronger when penetrating cytosine resulting the blue shift of ΔE_k. Furthermore, it should be noted that there are two counteracting influences on the collision process. On the one hand, the faster proton exposes higher frequency components to cytosine. On the other hand, the slower proton lengthens the interaction time, which leads to an enhanced reaction yield in turn. In Fig. 9, in the range of 150 eV $\leq E_k \leq$ 360 eV, when the incident energy of proton increases, the excitation becomes more violent even though the interaction time is shortened, implying that the enhancement by the higher frequency components dominates over increased interaction time. In the range of 360 eV $< E_k \leq$ 1000 eV, the excitation becomes less violent as the incident energy of proton increases, indicating that the interaction time dominates mainly. In addition, after systematic exploration, we find that the main dissociation pathway of cytosine is the breaks of C_1N_2 and N_8H_{10}. This corresponds well with the result found by Leila *et al.* that the initial bond cleavage of C_1N_2 is the main dissociation route.[15] Moreover, it is found that there is no bond breaking when the energy loss of proton is less than 22 eV.

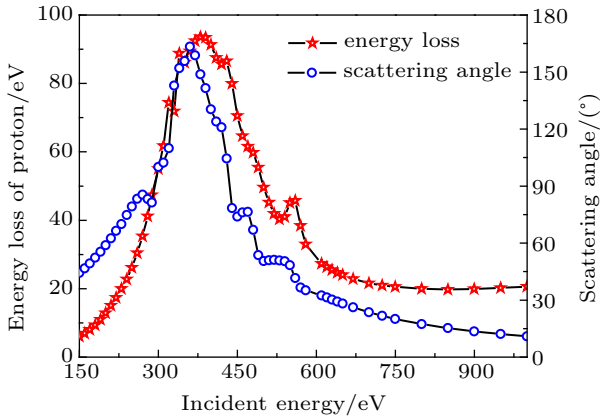

Fig. 9. The energy loss of proton (left Y axis) and the scattering angle of proton (right Y axis) as a function of the incident energy of proton.

4. Conclusion

In summary, we have studied both the static properties and the collision dynamics of cytosine by proton impact using the TDDFT-MD method. The calculated optimized ground state of cytosine accords well with experiments. We especially explore the effect of the incident energy of proton on the collision dynamics. Two typical collision reaction channels are exhibited by analyzing the molecular ionization, the electronic density evolution, the energy loss of proton and the scattering pattern. The results show that the proton captures some electrons, resulting in the decreases of the bonds C_3N_8 and C_5N_6 while the increases of the bonds C_4H_{11}, C_5H_{12} and C_4C_5. It is found that proton transfers maximum energy, about 23.9% of the incident energy, to cytosine when the incident kinetic energy is about 390 eV. The peak of the scattering angle shows a little red shift when compared to that of the loss of kinetic energy of proton. Furthermore, we find that proton is scattered in the present study and the dissociation of cytosine occurs when the energy loss of proton is larger than 22 eV, which is the breaks of C_1N_2 and N_8H_{10}.

It should be noted that the calculations presented here are exploratory. It is necessary to launch a comprehensive study to understand the collision precisely. However, it is not computationally feasible yet. This work aims at the study of the proton+cytosine collision problem using the TDDFT to see how a cytosine evolves during and after the impact of proton with energy ranging from 150 eV to 1000 eV. More effort should be devoted to employing the effects of the orientation and the larger energy on the collision dynamics of cytosine. Work along that direction is in progress.

References

[1] Von Sonntag C 2006 *Free-Radical-Induced DNA Damage and Its Repair* (Berlin: Springer)
[2] Baccarelli I, Gianturco F A, Scifoni E, Solov'yov A V and Surdutovich E 2010 *Eur. Phys. J. D* **60** 1
[3] Michael B D and O'Neill P 2000 *Science* **287** 1603
[4] Gonzalgo M L and Jones P A 1997 *Mutation Res.-Rev. Mutation Res.* **386** 107
[5] Shikazono N, Noguchi M, Fujii K, Urushibara A and Yokoya A 2009 *J. Radiat. Res.* **50** 27
[6] Poully J C, Miles J, De Camillis S, Cassimi A and Greenwood J B 2015 *Phys. Chem. Chem. Phys.* **17** 7172
[7] Plekan O, Feyer V, Richter R, Coreno M, de Simone M and Prince K C 2007 *Chem. Phys.* **334** 53
[8] Touboul D, Gaie-Levrel F, Garcia G A, Nahon L, Poisson L and Schwell M 2013 *J. Chem. Phys.* **138** 094203
[9] Tabet J, Eden S, Feil S, Abdoul-Carime H, Farizon B, Farizon M, Ouaskit S and Märk T D 2010 *Phys. Rev. A* **82** 022703
[10] Chen L, Bredy R, Bernard J, Montagne G, Allouche A R and Martin S 2011 *J. Chem. Phys.* **135** 114309
[11] Brédy R, Bernard J, Chen L, Wei B, Salmoun A, Bouchama T, Buchet-Poulizac M C and Martin S 2005 *Nucl. Instrum. Methods. Phys. Res. Sect. B* **235** 392
[12] Seraide R, Bernal M A, Brunetto G, De Giovannini U and Rubio A 2017 *J. Phys. Chem. B* **121** 7276
[13] Das T and Ghosh D 2014 *J. Phys. Chem. A* **118** 5323
[14] Dal Cappello C, Hervieux P A, Charpentier I and Ruiz-Lopez F 2008 *Phys. Rev. A* **78** 042702
[15] Sadr-Arani L, Mignon P, Chermette H, Abdoul-Carime H, Farizon B and Farizon M 2015 *Phys. Chem. Chem. Phys.* **17** 11813
[16] Chen Z Y, Lau K C, Garcia G A, Nahon L, Božanić D K, Poisson L, Al-Mogren M M, Schwell M, Francisco J S, Bellili A and Hochlaf M 2016 *J. Am. Chem. Soc.* **138** 16596
[17] Trofimov A B, Schirmer J, Kobychev V B, Potts A W, Holland D M P and Karlssons L 2006 *J. Phys. B: At. Mol. Opt. Phys.* **39** 305
[18] Le Padellec A, Moretto-Capelle P, Richard-Viard M, Champeaux J P and Cafarelli P 2008 *J. Phys.: Conf. Ser.* **101** 012007
[19] Rice J M, Dudek G O and Barder M 1965 *J. Am. Chem. Soc.* **87** 4569
[20] Wolken J K, Yao C X, Tureček F, Polce M J and Wesdemiotis C 2007 *Int. J. Mass Spectrom.* **267** 30
[21] See http://pw-teleman.org/ for the information about the TDDFT-MD model.
[22] Calvayrac F, Reinhard P G, Suraud E and Ullrich C A 2000 *Phys. Rep.* **337** 493
[23] Fennel Th, Meiwes-Broer K H, Tiggesbäumker J, Reinhard P G, Dinh P M and Suraud E 2010 *Rev. Mod. Phys.* **82** 1793
[24] Dinh P M, Reinhard P G and Suraud E 2010 *Phys. Rep.* **485** 43
[25] Zhao R T, Zhang N and Zhang F S 2018 *Mol. Phys.* **116** 231
[26] Yu W, Gao C Z, Zhang Y, Zhang F S, Hutton R, Zou Y and Wei B 2018 *Phys. Rev. A* **97** 032706
[27] Hong X H, Wang F, Wu Y, Gou B C and Wang J G 2016 *Phys. Rev. A* **93** 062706
[28] Wang Z P, Dinh P M, Reinhard P G, Suraud E, Bruny G, Montano C, Feil S, Eden S, Abdoul-Carime H, Farizon B, Farizon M, Ouaskit S and Märk T D 2009 *Int. J. Mass. Spectrom.* **285** 143
[29] Krasheninnikov A V, Miyamoto Y and Tománek D 2007 *Phys. Rev. Lett.* **99** 016104
[30] Miyamoto Y and Zhang H 2008 *Phys. Rev. B* **77** 165123
[31] Wang Z P, Dinh P M, Reinhard P G, Suraud E and Zhang F S 2011 *Int. J. Quantum. Chem.* **111** 480
[32] Ndongmouo-Taffoti U F, Dinh P M, Reinhard P G, Suraud E and Wang Z P 2010 *Eur. Phys. J. D* **58** 131
[33] Gaigeot M P, Lopez-Tarifa P, Martin F, Alcami M, Vuilleumier R, Tavernelli I, Hervé du Penhoat M A and Politis M F 2010 *Mutation Res.-Rev. Mutation Res.* **704** 45
[34] Marques M A L and Gross E K U 2004 *Annu. Rev. Phys. Chem.* **55** 427
[35] Goedecker S, Teter M and J Hutter 1996 *Phys. Rev. B* **54** 1703
[36] Perdew J P and Wang Y 1992 *Phys. Rev. B* **45** 13244
[37] Legrand C, Suraud E and Reinhard P G 2002 *J. Phys. B* **35** 1115
[38] Ullrich C A 2000 *J. Mol. Struct. (THEOCHEM)* **501-502** 315
[39] Gao C Z, Wang J, Wang F and Zhang F S 2014 *J. Chem. Phys.* **140** 054308
[40] Barker D L and Marsh R E 1964 *Acta Cryst.* **17** 1581
[41] Improta R, Scalmani G and Barone V 2000 *Int. J. Mass. Spectrom.* **201** 321
[42] Hush N S and Cheung A S 1975 *Chem. Phys. Lett.* **34** 11
[43] Tehrani Z A, Javan M J, Fattahi A and Hashemi M M 2012 *J. Theor. Comput. Chem.* **11** 313
[44] Radchenko E D, Sheina G G, Smorygo N A and Blagoi Yu P 1984 *J. Mol. Struct.* **116** 387
[45] Susi H, Ard J S and Purcell J M 1973 *Spectrochim. Acta* **29A** 725